PLASTICITY MODEL FOR SAND UNDER SMALL AND LARGE CYCLIC STRAINS

By Archilleas G. Papadimitriou,[1] George D. Bouckovalas,[2] and Yannis F. Dafalias,[3] Members, ASCE

ABSTRACT: A plasticity constitutive model for sands is proposed, which combines a bounding surface framework for large cyclic strains with a Ramberg-Osgood-type hysteretic formulation for relatively smaller strains. The distinction between small and large cyclic strains is based on the volumetric threshold cyclic shear strain γ_{tv}, a well-established geotechnical parameter. The state parameter ψ is used explicitly to interrelate the critical, peak, and dilatancy deviatoric stress ratios. The plastic modulus is expressed as a particular function of accumulated plastic volumetric strain, which simulates empirically the effect of fabric evolution during shearing. Extensive comparisons with experiments show accurate simulation of the basic aspects of cyclic behavior for a wide range of cyclic strain amplitudes, specifically, (1) the degradation of shear modulus and increase of hysteretic damping with cyclic shear strain amplitude; (2) the evolving rates of shear strain and excess pore pressure (or volumetric strain) accumulation with number of cycles; and (3) the resistance to liquefaction. The 14 model parameters are proven independent of initial and drainage conditions, as well as the cyclic shear strain amplitude. The simulation of monotonic shearing is equally accurate.

INTRODUCTION

Currently available analytical models of sand behavior have captured qualitatively most features of the measured stress-strain relations. Nevertheless, quantitative accuracy is still an issue, especially for cyclic shearing [e.g., Popescu and Prevost (1995)]. In fact, most formulations require readjustment of parameters in order to predict accurately the effect of initial state (i.e., relative density and effective stress level) on shear behavior, or the basic aspects of cyclic response under variable cyclic shear strain amplitudes.

Simulating the effect of initial state with a single set of model parameters has proven difficult for analytical models built strictly within the classical framework of critical state soil mechanics (CSSM) [e.g., Schofield and Wroth (1968)]. Two key alterations had to be introduced to the CSSM framework for this purpose:

- Departure from the κ-λ idealization of consolidation behavior, by allowing for model predicted, and not user defined, normal consolidation lines with slopes depending on initial conditions [e.g., Jefferies (1993), Manzari and Dafalias (1997), and Gajo & Wood (1999)].
- Direct association of shear behavior to the state parameter ψ (Been and Jefferies 1985), which is defined with respect to a unique critical state line (CSL) or steady state line. In particular, introduction of ψ in constitutive equations has been achieved both implicitly (Jefferies 1993) and explicitly (Manzari and Dafalias 1997; Gajo and Wood 1999; Li et al. 1999; Li and Dafalias 2000).

Cyclic shearing has been addressed in constitutive modeling literature mostly via kinematic hardening, which appropriately extends the application of otherwise monotonic formulations. Thus, little attention is given to accurate simulation of basic behavioral patterns observed in cyclic shearing alone, such as hysteresis and plastic strain accumulation with a number of cycles. In fact, there is no evidence in the literature of model formulations that can provide quantitative accuracy for small and large cyclic shear strain amplitudes with a single set of parameters. Note that the terms ''small'' and ''large'' cyclic strains in this paper describe sand behavior merely from an experimental point of view. In other words, there is no intention to address nonlinear effects due to large displacements and rotations (geometric nonlinearity).

The constitutive model presented herein has been developed with the aim to overcome the foregoing shortcomings. It builds upon the recent critical state elastoplastic model by Manzari and Dafalias (1997) that accounts efficiently for different initial states with a single set of parameters and incorporates two new key features. First, the introduction of small strain nonlinear hysteretic response, as a substitute for the traditionally elastic (or hypoelastic) response at small cyclic strain amplitudes, in a manner similar to the paraelastic theory of Hueckel and Nova (1979). Second, the use of a properly defined scalar-valued variable, which reflects macroscopically the effect of fabric evolution during shearing on the plastic modulus. Both new features have been formulated in close accordance with experimental evidence from a wide variety of cyclic test conditions.

In the following presentation, equations that originate from Manzari and Dafalias (1997) are not fully elaborated so that the framework of sand behavior and the new features of the formulation can be highlighted. To address nonexpert geotechnical engineers, constitutive equations are presented in the simplifying triaxial stress-strain space. For completeness, the basic concepts of their generalization in the multiaxial space are presented in a dedicated paragraph. The triaxial stress components used for this purpose are the mean effective $p = 1/3(\sigma_v + 2\sigma_h)$ and the deviatoric stress $q = \sigma_v - \sigma_h$, where subscripts v and h denote the vertical and horizontal directions, respectively. Similarly, the triaxial strain components are the volumetric $\varepsilon_p = \varepsilon_v + 2\varepsilon_h$ and the deviatoric strain $\varepsilon_q = 2/3(\varepsilon_v - \varepsilon_h)$.

BEHAVIORAL PATTERN FOR SANDS

It is well documented that continuing monotonic shearing of sand eventually leads to a critical state. Denser than critical

[1]Res. Assoc., Dept. of Geotech. Engrg., Facu. of Civ. Engrg., Nat. Tech. Univ. of Athens, Athens 10682, Greece (corresponding author). E-mail: loupapas@alum.mit.edu

[2]Assoc. Prof., Dept. of Geotech. Engrg., Facu. of Civ. Engrg., Nat. Tech. Univ. of Athens, Athens 10682, Greece. E-mail: g.bouck@civil.ntua.gr

[3]Prof., Dept. of Mech., Facu. of Appl. Math. and Phys. Sci., Nat. Tech. Univ. of Athens, Zographou 15773, Greece, and Prof., Dept. of Civ. and Envir. Engrg., Univ. of California, Davis, CA 95616. E-mail: yfdafalias@ucdavis.edu

Note. Discussion open until April 1, 2002. To extend the closing date one month, a written request must be filed with the ASCE Manager of Journals. The manuscript for this paper was submitted for review and possible publication on February 22, 2000; revised May 18, 2001. This paper is part of the ***Journal of Geotechnical and Geoenvironmental Engineering***, Vol. 127, No. 11, November, 2001. ©ASCE, ISSN 1090-0241/01/0011-0973–0983/$8.00 + $.50 per page. Paper No. 22288.

states of sand tend to dilate under shear for sufficiently large values of the deviatoric stress ratio q/p, while initially looser states tend to contract for any value of q/p. This gradual change from dilative to contractive behavior can be quantified in terms of the state parameter ψ (Been and Jefferies 1985), defined with respect to a unique CSL in the e-p space. By assuming a linear relation for the CSL in the e-ln(p) space, ψ takes the following form:

$$\psi = e - e_{CS} = e - (e_{CS})_a + \lambda \ln\left(\frac{p}{p_a}\right) \quad (1)$$

where λ and $(e_{CS})_a$ = parameters defining the location of the CSL; and p_a = atmospheric pressure (e.g., p_a = 98.1 kPa). Hence, a tendency for contraction is expected for positive ψ values, while a tendency for dilation is related to negative ψ and sufficiently large values of q/p.

For cyclic shearing, behavior is also influenced by the single amplitude cyclic shear strain level γ_c [e.g., Vucetic (1994)]. For practical purposes, this behavior may be grossly described with reference to a unique threshold strain γ_{tv}, as follows:

- For small cyclic strains ($\gamma_c \leq \gamma_{tv}$), the secant shear modulus G_s degrades from its initial value G_{max} with increasing γ_c, while the hysteretic damping ratio ξ increases with respect to its initial value $\xi_{min}(\neq 0)$. For this cyclic strain range, minor accumulation of plastic strain or excess pore pressure is observed, especially for a small number of cycles N (e.g., earthquake-induced shearing).
- For large cyclic strains ($\gamma_c > \gamma_{tv}$), G_s and ξ are very different from their initial values, while the phenomena of permanent strain accumulation and excess pore pressure buildup become dominant. Therefore, N plays a key role in describing cyclic behavior.

According to Vucetic (1994), for sands and nonplastic silts (I_P = 0%) the volumetric cyclic threshold strain γ_{tv} usually takes values between 0.0065 and 0.025%.

Sand fabric (i.e., the orientation of particle contact planes) evolves during shearing. For example, Oda et al. (1985) show that the normal to particle contact plane reorients itself during monotonic shearing and tends to become coaxial with the major principal stress. This evolution of fabric ceases only at critical state. Of interest to this paper is the effect of fabric evolution during shearing on the measured stress-strain response, especially during shear unloading and reloading.

Laboratory data show that if shearing is reversed at its early stages (i.e., below a threshold shear stress), shear unloading is stiff and leads to partly reversed fabric and volume changes [e.g., Chen et al. (1988)]. Reloading in the original direction is stiffer, since density has increased slightly and some particle contacts have remained realigned toward the direction of the major principal stress of the original shearing [e.g., Arthur et al. (1981)]. Such observations explain why successive drained shear cycles of relatively small amplitude lead to a continuously stiffening unloading-reloading response [e.g., Ladd et al. (1977)]. When the shear cycles are of larger amplitude, the unloading paths, in particular, become significantly compliant [e.g., Ladd et al. (1977)]. Ishihara et al. (1975) showed that such relatively compliant unloading is observed only when the shear reversal point is beyond the phase transformation line (PTL) and dilation took place before unloading. Hence, the PTL can successfully play the role of a threshold in stress space that can alter the stress-strain response due to volumetric changes and fabric evolution during shearing.

To demonstrate macroscopically these effects, Fig. 1 presents typical results from an undrained cyclic triaxial test [data from Arulmoli et al. (1992)]. It is shown that the average rate of excess pore pressure Δu buildup decreases gradually at the initial stage of shearing (for cycles N = 1–31) and increases thereafter, as the soil approaches liquefaction. Observe that this gradual increase in Δu buildup is mainly due to more compliant unloading, since reloading is considerably stiffer (compare paths 2–3 and 4–5). Furthermore, the unloading response becomes gradually more compliant as the distance of the shear reversal point above the PTL becomes larger (compare paths b–c, 2–3, and 6–7). This evolution of the average rate is typical for Δu [e.g., Seed and Booker (1977)] and has also been observed for permanent strain accumulation (Egglezos and Bouckovalas 1999).

It is customary to treat fabric as a directional property. Nevertheless, based on the above, its relation to dilative or contractive behavior allows for a simplifying approach to account for the effect of fabric evolution during shearing via a scalar-valued variable.

MODEL OUTLINE

The proposed yield/bounding surface formulation assumes a user defined and unique CSL in the e-p space, a traditional assumption for critical state models. Departing from such formulations, the normal consolidation line of the proposed model is neither unique nor user defined but is model predicted depending on initial conditions. As shown in Fig. 2, the yield surface has the form of an open wedge with the apex at the origin of axes, and its yield function is given by (Manzari and Dafalias 1997)

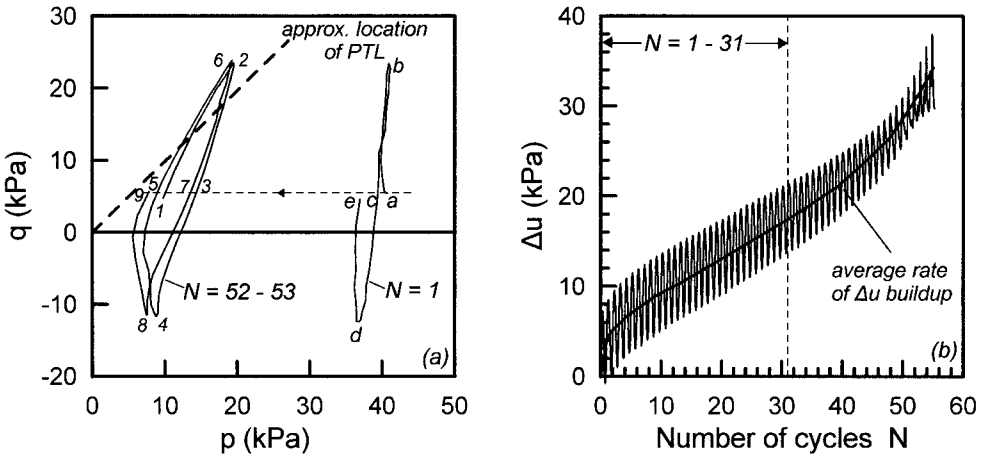

FIG. 1. Typical Cyclic Liquefaction Triaxial Test Results [Data from Arulmoli et al. (1992)]: (a) Selected Cycles in p-q Space; (b) Rate of Δu Buildup as Function of N

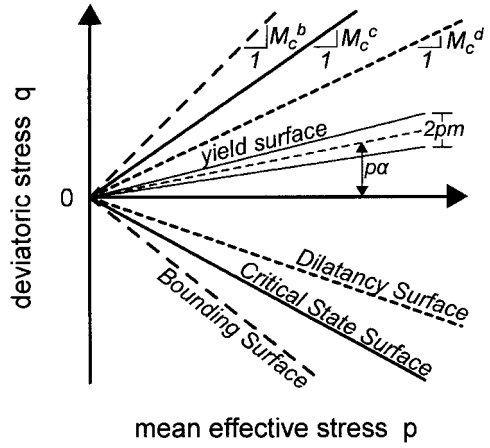

FIG. 2. Model Surfaces in *p-q* Space

$$f = \frac{q}{p} - \alpha \mp m = \eta - \alpha - sm = 0 \tag{2}$$

where $\eta = q/p$ = deviatoric stress ratio; and scalars m and α = tangents of angles related to the opening and the location of the bisector of the yield surface, respectively. While m remains constant throughout shearing, the value of α changes for shear paths that cause plastic strains. In other words, isotropic hardening is neglected, while kinematic hardening is incorporated via the evolution of α. Scalar s is an auxiliary parameter taking the value of $s = +1$ when $(\eta - \alpha) \geq 0$, and $s = -1$ in the opposite case. Hence, its use in (2) replaces the cumbersome $\pm$ sign, a useful analytical tool for subsequent equations as well.

Besides the yield surface, the model incorporates the use of three more surfaces: the critical state, bounding, and dilatancy surfaces. As shown in Fig. 2, all three surfaces have the form of open wedges with the apex at the origin of the *p-q* axes. Their shape for triaxial compression is fully defined by slopes M_c^c, M_c^b, and M_c^d (collectively $M_c^{c,b,d}$). Similarly, their shape for triaxial extension is fully defined by slopes $M_e^{c,b,d}$. Following Manzari and Dafalias (1997), slopes $M_{c,e}^c$ are constant model parameters. On the contrary, $M_{c,e}^b$ and $M_{c,e}^d$ are continuous functions of $M_{c,e}^c$ and the ever-changing value of the state parameter ψ as

$$M_{c,e}^b = M_{c,e}^c + k_{c,e}^b \langle -\psi \rangle \tag{3}$$

$$M_{c,e}^d = M_{c,e}^c + k_{c,e}^d \psi \tag{4}$$

where $k_{c,e}^b$ and $k_{c,e}^d$ = model parameters and $\langle\ \rangle$ are the Macauley brackets yielding $\langle A \rangle = A$ if $A > 0$ and $\langle A \rangle = 0$ if $A \leq 0$. It is noted that (3) without the Macauley brackets was first proposed by Wood et al. (1994). Although $M_{c,e}^{b,d}$ dependence on ψ could be more complicated for greater accuracy [e.g., Li et al. (1999) and Li and Dafalias (2000)], the linear form of (3) and (4) is considered adequate for the present needs.

The strain increment $d\varepsilon_{p,q}$ is deconvoluted into $d\varepsilon_{p,q}^e$ and $d\varepsilon_{p,q}^p$, the elastic and the plastic components. Alternative subscripts p and q denote the volumetric and deviatoric parts of each strain component. For any effective stress increment (dp, dq), the elastic strains are given by

$$d\varepsilon_q^e = \frac{dq}{3G_t} \tag{5a}$$

$$d\varepsilon_p^e = \frac{dp}{K_t} \tag{5b}$$

where K_t and G_t = tangential bulk and shear moduli, respectively. The plastic strain components are given by

$$d\varepsilon_q^p = s\sqrt{\frac{2}{3}}\langle L \rangle \tag{6a}$$

$$d\varepsilon_p^p = D\left|d\varepsilon_q^p\right| \tag{6b}$$

where the scalar D = dilatancy coefficient used to define the flow rule of the formulation, and the scalar L = loading index, given by

$$L = s\frac{p}{K_p}d\eta \tag{7}$$

In (7), $d\eta$ is the incremental change of the deviatoric stress ratio $\eta = q/p$, and K_p is the plastic modulus. Note that the Macauley brackets in (6) ensure that nonpositive values of L lead to $d\varepsilon_{p,q}^p = 0$. Practically, the sign of L determines the loading conditions: $L > 0$ for loading, $L < 0$ for unloading, and $L = 0$ for neutral loading.

Based on the above, it becomes possible to define the kinematic hardening of the formulation, which is expressed in terms of the yield surface axis movement in stress space via the scalar increment $d\alpha$. This scalar increment corresponds to the change in value of the tangent of angle α [i.e., the angle locating the bisector of the yield surface (Fig. 2)]. The consistency condition $df = 0$ applied to (2) yields $d\alpha = d\eta$, which in conjunction with (7) yields

$$d\alpha = s\left(\frac{K_p}{p}\right)\langle L \rangle \tag{8}$$

Eqs. (5)–(8) outline the incremental stress-strain relations of the proposed model in the triaxial space and require specific forms for parameters K_t, G_t, D, and K_p. These are provided in subsequent paragraphs, where use of (1), (3), and (4) is explicitly made. Numerical integration of the stress-strain relations is performed through a simple forward scheme, in which K_t, G_t, D, and K_p are assumed constant over a small increment of stress or strain, equal to their values at the beginning of the increment.

ELASTIC STRAIN CALCULATION

Departing from Manzari and Dafalias (1997), the tangential elastic moduli K_t and G_t are interrelated via a constant elastic Poisson's ratio ν. Furthermore, G_t decreases smoothly during shearing similarly to the widely used nonlinear hysteretic stress-strain relation of Ramberg and Osgood (1943). In particular, the tangent shear modulus is expressed as

$$G_t = \frac{G_{\max}}{T} \tag{9}$$

The maximum value of shear modulus $G_{\max}$ is given by a generalization of the well-established formula of Hardin (1978) as

$$G_{\max} = \frac{Bp_a}{0.3 + 0.7e^2}\left(\frac{p}{p_a}\right)^{0.5} \tag{10}$$

where B = model parameter. The value of scalar T is given by

$$T = \left\{\begin{array}{l} 1 + 2\left(\frac{1}{a_1} - 1\right)\left(\frac{|\eta - \eta_o|}{\eta_1}\right), \text{ first loading} \\ 1 + 2\left(\frac{1}{a_1} - 1\right)\left(\frac{|\eta - \eta_{SR}|}{2\eta_1}\right), \text{ unload and reload} \end{array}\right\}$$
$$\leq 1 + 2\left(\frac{1}{a_1} - 1\right) \tag{11}$$

where η_{SR} and η_o = deviatoric stress-ratios at the last shear reversal (SR) and at consolidation, respectively. Scalars a_1 and η_1 are parameters whose physical meaning will be described

below. SR for the elastic strain formulation is defined at a point where the deviatoric strain increment $d\varepsilon_q$ changes sign (i.e., when $[d\varepsilon_q^{(i)}\ d\varepsilon_q^{(i-1)}] < 0$, where $(i-1)$ and (i) denote successive steps in the forward integration scheme). It should be noted that an SR point, defined as above, does not necessarily correspond to a point of change in loading conditions defined by a change in the sign of L. For example, this is true for an SR point within the yield surface.

Observe that the elastic strain increments calculated by (9)–(11) are not fully recoverable (i.e., the proposed elastic strain formulation is not literally elastic). According to Hueckel and Nova (1979), a better term for such formulations is paraelastic. Nevertheless, the term ''elastic'' is maintained in this paper as a reminder that (9)–(11) apply to all stress states, within as well as on the yield surface, similarly to elastic strains estimated by traditional elastoplastic models. Thus, the yield surface merely includes stress states with $d\varepsilon_{p,q}^{p} = 0$ and is not the boundary of purely elastic states (i.e., there is no purely elastic region in this model).

Physical insight to the proposed elastic model is gained for an ideal case of shearing under constant $G_{\max} = G_{\max}^{o}$ (i.e., its value at consolidation). Under this assumption (i.e., by overlooking any changes in p and e), (9)–(11) may be analytically integrated. Fig. 3 presents the stress-strain relation for a monotonic test and a cyclic drained constant-p triaxial test, which were estimated analytically according to this procedure. Observe that the monotonic path for $\eta < \eta_1$ is characterized by a smooth degradation of G_t from $G_{\max}^{o}$ to $G_{\min}^{o}$. As a result of the inequality in (11), for larger stresses and strains, the tangential modulus G_t remains equal to the constant value of $G_{\min}^{o} = G_{\max}^{o}/[1 + 2(1/a_1 - 1)]$.

For the shear loop of Fig. 3, which is characterized by a deviatoric stress ratio amplitude $\eta_c \le \eta_1$, analytical integration leads to the following expression for the secant shear modulus ratio $G_s/G_{\max}^{o}$:

$$\frac{G_s}{G_{\max}^{o}} = \frac{1}{1 + \left(\frac{1}{a_1} - 1\right)\left(\frac{\eta_c}{\eta_1}\right)} \tag{12}$$

Since $\eta_c = 2(G_s/G_{\max}^{o})(G_{\max}^{o}/p_o)\gamma_c$ and $\eta_1 = 2a_1(G_{\max}^{o}/p_o)\gamma_1$, (12) may be alternatively written in terms of γ_c and γ_1 as

$$\frac{G_s}{G_{\max}^{o}} = \frac{-1 + \sqrt{1 + 4g_c}}{2g_c} \tag{13a}$$

where

$$g_c = \frac{1 - a_1}{a_1^2}\left(\frac{\gamma_c}{\gamma_1}\right) \tag{13b}$$

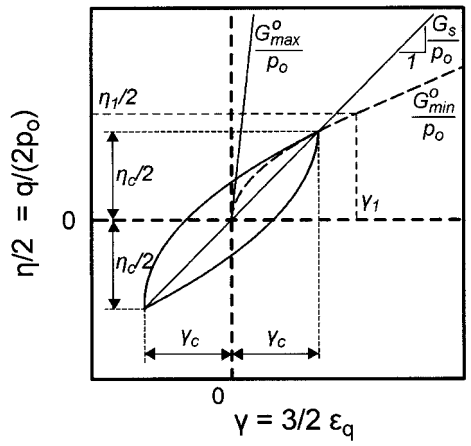

FIG. 3. Analytical Estimation of Elastic Deviatoric Stress-Strain Relation ($G_{\max}$ = Const)

Based on (13) it is deduced that $G_s/G_{\max}^{o} = a_1$ for $\gamma_c = \gamma_1$. Thus, a decrease of a_1 leads to increased nonlinearity. In general, since $G_t = G_{\min}$ for $\gamma > \gamma_1$, the model parameter γ_1 may be interpreted as a threshold strain beyond which the plastic component of strain dominates the behavior. Given that γ_{tv} is the threshold of cyclic shear strain beyond which strain accumulation during cyclic shearing becomes significant (Vucetic 1994), it is reasonable to assume that γ_1 is equal to γ_{tv}.

The fixed size of the yield surface, quantified by m, has yet to be defined. Its only purpose is to lead to a relatively small, but distinguishable for numerical purposes, yield surface. Application of the model has shown that a value of m equal to $0.05M_c^c$ is considered appropriate for this purpose.

From all of the above, it is deduced that the proposed elastic model can be directly related to experimental data and is thus considered insightful for geotechnical engineers. On the other hand, it is nonconservative since it does not lead to recoverable strains. Nevertheless, the assumed small size of the yield surface is expected to ensure relatively small numerical difficulties in boundary-value problems.

PLASTIC STRAIN CALCULATION

Following the basic concepts of bounding surface plasticity theory [e.g., Dafalias and Popov (1975)], the dilatancy coefficient D and the plastic modulus K_p are adjusted according to the ''distance'' of the current stress state with respect to a ''conjugate'' stress state on the corresponding model surfaces. Fig. 4 shows the shape of the model surfaces in (p, η) space, where $\eta = q/p$, and defines the conjugate stress states. In the case of compression (i.e., $s = +1$), the conjugate stress state of (p, η) is $(p, M_c^{c,b,d})$, while in the case of extension (i.e., $s = -1$) the conjugate is $(p, -M_e^{c,b,d})$. In general, the ordinates $M^{c,b,d}$ of the conjugate points on the critical state, bounding, and dilatancy surfaces are given as

$$M^{c,b,d} = s(M_c^{c,b,d}\langle s\rangle + M_e^{c,b,d}\langle -s\rangle) \tag{14}$$

The scalar distances $d^{c,b,d}$ between the current and the conjugate stress states in (p, η) space are given as

$$d^{c,b,d} = s(M^{c,b,d} - \eta) \tag{15}$$

The dilatancy coefficient D in (6b) is related to the distance from the dilatancy surface d^d (Manzari and Dafalias 1997)

$$D = A_o d^d \tag{16}$$

In (16), A_o is a positive model parameter, so that the sign of D is solely associated to the sign of d^d. Thus, when loading ($L > 0$) continues beyond the dilatancy surface and distance d^d becomes negative, scalar D as well as the plastic volumetric strain $d\varepsilon_p^p$ resulting from (6b) become negative, hence, simulating dilative response. In this sense, the dilatancy surface

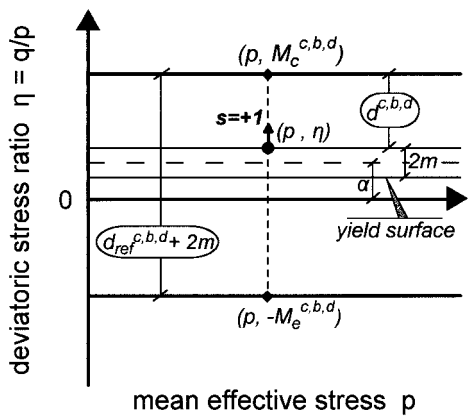

FIG. 4. Model Surfaces and Projection Rule in p-η Space

practically corresponds to the PTL established experimentally by Ishihara et al. (1975). Finally, to ensure that no dilation occurs in the unlikely case of $\psi > 0$ and $d^d < 0$, a limitation of $D = 0$ must be introduced until one of the two inequalities ceases to hold.

The plastic modulus K_p in (7) is related to the distance from the bounding surface d^b as

$$K_p = p h_b h_f d^b \tag{17}$$

The scalar parameters p, h_b, and h_f are nonnegative, so that the sign of K_p is governed by the sign of d^b. More specifically

$$h_b = h_o \frac{|d^b|}{\langle d^b_{ref} - |d^b| \rangle} \tag{18}$$

where h_o = positive model parameter. As shown in Fig. 4, d^b_{ref} is a "reference" distance corresponding to the distance between points (p, M^b_c) and $(p, -M^b_e)$ minus the "diameter" of the yield surface in the (p, η) space

$$d^b_{ref} = M^b_c + M^b_e - 2m \tag{19}$$

The scalar function h_f in (17) expresses macroscopically the effect of fabric evolution during shearing on the plastic modulus K_p and, in extent, on both the deviatoric and the volumetric components of plastic strain. In particular, h_f is defined as

$$h_f = \frac{1 + F \left\langle \int d\varepsilon^p_p(\%) \right\rangle^2}{1 + F \int_{SR_{-1}}^{SR} \langle -d\varepsilon^p_p(\%) \rangle} \tag{20}$$

where F = positive constant. To clarify the operation of function h_f, Fig. 5(a) presents a typical simulation of an undrained triaxial test including SRs. Observe that the integral in the numerator of (20) changes constantly during shear paths that cause plastic strains. As a result, the numerator increases gradually for stress paths that remain within the dilatancy surface, or under the PTL (path $1-c_1$), and starts to decrease only when shearing continues beyond it [i.e., when $d\varepsilon^p_p < 0$ (paths c_1-6 and c_2-8)]. However, even in such cases, the Macauley brackets in the numerator ensure that the numerator never becomes less than unity (i.e., its value at consolidation).

Unlike the constantly evolving numerator, the denominator of (20) changes only at each SR point. Hence, during monotonic shearing it remains equal to 1 (i.e., its value at consolidation). In all other cases, its value is a function of the negative plastic volumetric strain accumulated during the path between the last SR point and its antecedent SR_{-1}. For example, at each point during path 6–7 in Fig. 5(a), the value of the integral in the denominator is constant and corresponds to the negative plastic volumetric strain accumulated during path 5–6. Hence, for any point along path 6–7 points SR_{-1} and SR in (20) are points 5 and 6, respectively. Due to the included Macauley brackets, the denominator of (20) takes a value larger than 1, only when SR takes place beyond the dilatancy surface.

Although F in (20) could be taken constant (Papadimitriou et al. 1999), refined simulations can be obtained if it is correlated to the initial conditions (e_o, p_o) by

$$F = F_o \left(\frac{p_o}{p_a} \right)^{-X} \langle -\psi_o \rangle \tag{21}$$

where F_o and X = positive model parameters; and ψ_o = initial value of ψ. Observe that for initially contractive states ($\psi_o > 0$), the term inside the Macauley brackets in (21) becomes negative. Hence, the procuring value of F becomes zero, implying that the effect of fabric evolution during shearing is considered relatively significant to require analytical simulation only for sands in initially dilative states ($\psi_o < 0$). Similarly, the more dilative the initial state, the more important should the effect of fabric evolution be. Hence, the value of F increases with increasing $\langle -\psi_o \rangle$, as well as with decreasing p_o (due to the positive value of X).

To demonstrate the practical significance of the effect of fabric evolution, Fig. 5(b) presents another simulation of the shearing sequence of Fig. 5(a) for which the effect of fabric evolution during shearing is neglected (i.e., $F_o = 0$). Observe that taking into account the effect of fabric evolution during shearing leads to stiffening response for paths within the dilatancy surface [compare paths 1–5 in Figs. 5(a and b)]. This trend is reversed only upon unloading from points beyond the dilatancy surface [compare paths 6–7 and 8–9 in Figs. 5(a and b)]. In that case, accounting for the effect of fabric evolution leads to more compliant unloading response (i.e., higher excess pore pressures and a more rapid decrease of effective stresses). This type of response is experimentally identified as the onset of liquefaction during undrained cyclic shearing (Fig. 1), and it is its modeling that guarantees the accuracy of relevant analytical simulations.

GENERALIZATION TO MULTIAXIAL STRESS-STRAIN SPACE

For details on the generalization and especially for the tensorial stress-strain incremental equations, the reader is referred to Manzari and Dafalias (1997). This section provides the basic principle of the generalization and focuses on the new features introduced herein.

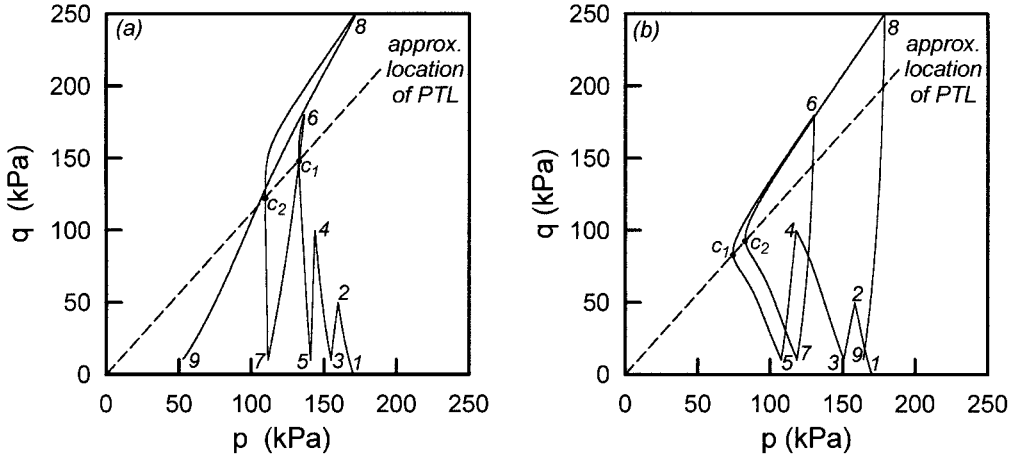

FIG. 5. Effect of Fabric Evolution during Shearing on Typical Simulations of Triaxial Stress Path for: (a) $F_o \neq 0$; (b) $F_o = 0$

As deduced from Fig. 4, the open wedge-type model surfaces in triaxial space are essentially defined in terms of deviatoric stress ratio values, independently of the value of p. This key role of η in triaxial space is being played by the deviatoric stress ratio tensor $\mathbf{r}_{ij}(=\mathbf{s}_{ij}/p)$ in multiaxial space, where $\mathbf{s}_{ij}$ is the deviatoric stress tensor. Hence, model surfaces in multiaxial stress space are essentially defined in terms of deviatoric stress ratio tensor values, independently of the value of p.

In the same manner, the role of deviatoric stress ratio differences $M^{c,b,d}$-η in the calculation of distances $d^{c,b,d}$ in p-q space is being played by the norm of the difference between the current deviatoric stress ratio tensor $\mathbf{r}_{ij}$ and appropriately defined conjugate deviatoric stress ratio tensors on the foregoing surfaces. Furthermore, traces of tensor products account properly by their signs for the change in generalized loading directions, an issue that was treated in the triaxial space by the use of scalar s, where $s = +1$ or $s = -1$ for triaxial compression and extension, respectively. Finally, the loading, unloading, and neutral loading conditions in multiaxial space are defined in terms of the sign of a scalar loading index L, similarly to their definition in the triaxial space.

Regarding the original features of this formulation, the scalar function h_f, which simulates the effect of fabric evolution during shearing, needs no generalization, since it takes into account plastic volumetric strain increments, which are also scalar values. On the other hand, generalization is necessary for the concept of shear reversal and the form of scalar parameter T, which provides nonlinearity to the elastic shear modulus G_t [(11)]. The latter will be addressed with the aid of an auxiliary scalar Q_r^{ref}

$$Q_r^{ref} = \sqrt{\frac{(\mathbf{r}_{ij} - \mathbf{r}_{ij}^{ref})(\mathbf{r}_{ij} - \mathbf{r}_{ij}^{ref})}{2/3}} \tag{22}$$

where $\mathbf{r}_{ij}^{ref}$ = value of the deviatoric stress ratio tensor $\mathbf{r}_{ij}$ at a reference state. In this manner, the scalar T in multiaxial space takes the following form:

$$T = \left\{ \begin{array}{l} 1 + 2\left(\frac{1}{a_1} - 1\right)\left(\frac{Q_r^o}{\eta_1}\right), \text{ first loading} \\ 1 + 2\left(\frac{1}{a_1} - 1\right)\left(\frac{Q_r^{SR}}{2\eta_1}\right), \text{ unload and reload} \end{array} \right\}$$
$$\leq 1 + 2\left(\frac{1}{a_1} - 1\right) \tag{23}$$

where scalar Q_r^o denotes the change in $\mathbf{r}_{ij}$ from its initial value at consolidation (where $\mathbf{r}_{ij} = \mathbf{r}_{ij}^o$) based on the general form of (22), while Q_r^{SR} similarly denotes the change in $\mathbf{r}_{ij}$ from its value at the last SR (where $\mathbf{r}_{ij} = \mathbf{r}_{ij}^{SR}$). Note that the scalar η_1 in (23) retains the form of η_1 used in (11) (i.e., it is a function of model parameters a_1 and γ_1 as well as G_{max}^o, the initial value of G_{max} at consolidation).

SR in the multiaxial stress space is defined with the aid of scalar Q_e^{SR}

$$Q_e^{SR} = \sqrt{\frac{(\mathbf{e}_{ij} - \mathbf{e}_{ij}^{SR})(\mathbf{e}_{ij} - \mathbf{e}_{ij}^{SR})}{2/3}} \tag{24}$$

where $\mathbf{e}_{ij}^{SR}$ = value of the deviatoric strain tensor $\mathbf{e}_{ij}$ at the last SR in history. In particular, shear reversal is defined at the point where dQ_e^{SR} changes sign (i.e., where the increment of scalar Q_e^{SR} changes sign).

PARAMETER CALIBRATION

The proposed model requires the calibration of 14 parameters. The full list is presented in Table 1, along with their typical range for the cyclic behavior of different sands, based on the literature and the writers' experience. The eleven first parameters in Table 1 can be rated directly from in situ and laboratory tests, while the remaining three (h_o, F_o, X) must be rated indirectly via trial-and-error simulations of laboratory tests. Details on the calibration procedure will be presented with reference to the Nevada sand database (Arulmoli et al. 1992), which is also used for assessing model performance in the next paragraph. In particular, model calibration is a step-by-step procedure initiating from the directly ratable parameters:

TABLE 1. Values of Model Parameters for Cyclic Shearing of Nevada Sand and Range of Values for Typical Sands

Parameter	Nevada sand	Typical sands
$(e_{CS})_a$	0.809	0.72 ÷ 0.90
λ	0.022	0.01 ÷ 0.03
M_c^c	1.25	1.20 ÷ 1.32
B	520[a]	500. ÷ 900.
a_1	0.67	0.45 ÷ 0.85
γ_1 (%)	0.025	0.0065% ÷ 0.025
m	0.0625	0.06 ÷ 0.07
ν	0.31	0.2 ÷ 0.4
k_c^b	1.45	0.8 ÷ 3.0
k_c^d	0.3	0.1 ÷ 3.0
A_o	2.1	1.0 ÷ 3.0
h_o	5,000	1,000 ÷ 10,000
F_o	100,000	100,000 ± 20,000
X	2.2	2.0 ± 0.3

[a]For monotonic shearing, $B = 200$.

- Critical state parameters $(e_{CS})_a$, λ, and M_c^c—These parameters are common in CSSM models, and, as usual, their calibration requires monotonic element tests that approach critical state. Evaluation of the available data for Nevada sand leads to $(e_{CS})_a = 0.809$, $\lambda = 0.022$, and $M_c^c = 1.25$.
- G_{max} parameter B—A value of B for cyclic shearing is estimated by fitting (10) to G_{max} measurements from independent small strain tests, such as resonant column or bender element tests. The Nevada sand database contains data of the former, and, according to Fig. 6(a), this procedure leads to $B = 520$. Values of B procuring from small strain measurements are usually too large for accurate simulation of monotonic shearing. In particular, values 2 to 3 times smaller are usually more appropriate. More specifically, a good estimate of B for monotonic shearing is obtained by fitting (10) to the initial stages of the deviatoric stress-strain relation of triaxial tests. Hence, according to Fig. 6(b) a value of $B = 200$ was selected for monotonic shearing of Nevada sand.
- G_s/G_{max} degradation parameters a_1 and γ_1—Their values are estimated on the basis of resonant column test data. In principle, an appropriate set of (a_1, γ_1) is one that fits (13) to the available data for $\gamma_c < \gamma_1$. As a guide, γ_1 should be taken equal to γ_{tv}, which ranges between 0.0065 and 0.025% for sands. Following this procedure, the pair of $(a_1, \gamma_1) = (0.67, 0.025\%)$ was selected to fit the data for Nevada sand [Fig. 6(c)].
- State dependence parameters k_c^b and k_c^d—Calibrating these parameters requires monotonic compression tests. A good estimate can be obtained by plotting the peak and the dilatancy deviatoric stress ratios η_{peak} and η_{dil} of different tests versus the respective initial values of the state parameter ψ_o. For instance, the plot of η_{peak} versus ψ_o for Nevada sand is shown in Fig. 6(d), leading to $k_c^b = 1.45$. A similar procedure for k_c^d leads to a value of 0.30.
- Elastic Poisson's ratio ν—This parameter affects the value of the elastic bulk modulus K_t, which procures indirectly from G_t and ν. An appropriate value can be es-

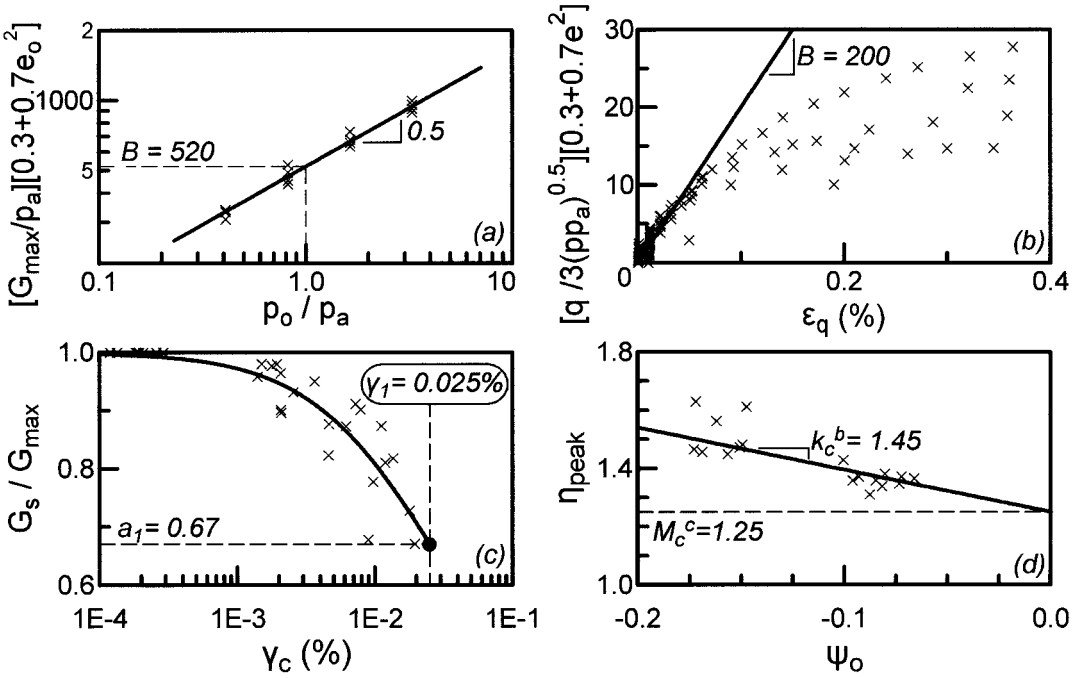

FIG. 6. Parameter Calibration of: (a) B for Cyclic Shearing from G_{max} Measurements; (b) B for Monotonic Shearing from Triaxial Tests; (c) a_1, γ_1 from G_s/G_{max}-γ_c Data; (d) k_c^b from Monotonic Triaxial Tests

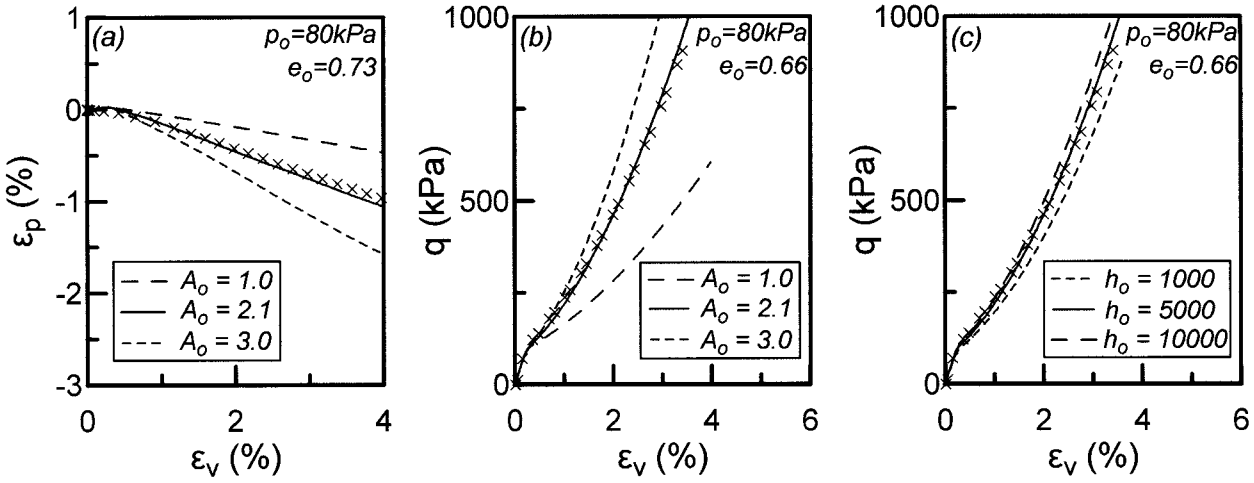

FIG. 7. Parameter Calibration and Sensitivity of Monotonic Shearing Simulations to Parameters A_o and h_o

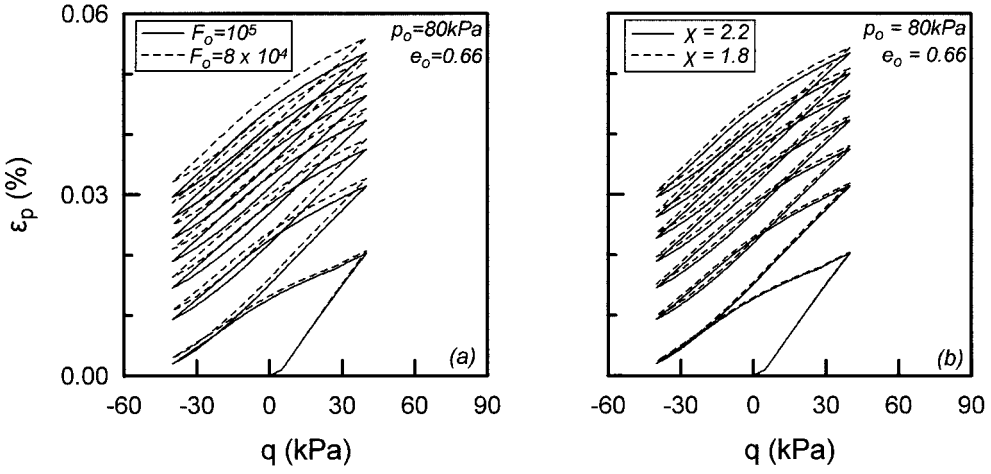

FIG. 8. Parameter Calibration and Sensitivity of Drained Cyclic Shearing Simulations to Parameters: (a) F_o; (b) X

timated from small strain measurements (e.g., crosshole), or from the initial stages of 1D unloading with lateral stress measurements (e.g., in a triaxial apparatus).
- Dilatancy constant A_o—The direct estimation of A_o requires good quality stress-dilatancy data (e.g., the results of volumetric strain ε_p versus deviatoric strain ε_q in a constant-p drained triaxial test).

For the remaining parameters, the trial-and-error sequence is initiated by selecting a representative couple of monotonic triaxial compression tests, one drained and one undrained, to act as the target stress-strain response. Simulations are initiated by setting $m = 0.0625$ (i.e., $m = 0.05M_c^c$) and by selecting typical values for h_o, F_o, and X from Table 1. Pinpointing values for F_o and X is of little practical importance for monotonic shearing. Thus, the trial-and-error sequence essentially refers to parameter h_o and possibly to directly ratable parameters, which could not be defined properly due to lack of relevant data. For Nevada sand in particular, the values of $h_o = 5{,}000$, $A_o = 2.1$, and $\nu = 0.31$ were estimated in this manner.

Model calibration ends by pinpointing F_o and X. This is achieved by performing trial-and-error simulations of cyclic triaxial tests with distinctly different initial conditions. For this purpose, two representative tests have to be selected as target stress-strain response.

To ascertain the sensitivity of simulations to usually indirectly rated model parameters, Figs. 7 and 8 compare appropriate parametric simulations for monotonic and cyclic shearing, respectively. In particular, Fig. 7 presents a parametric analysis for the effects of A_o and h_o on the simulated monotonic triaxial compression behavior [Fig. 7(a) for drained and Figs. 7(b and c) for undrained conditions]. Solid lines in Fig. 7 correspond to model simulations performed with the parameters of Table 1 for monotonic shearing, while the dashed lines correspond to the noted parametric runs. Observe that appropriate calibration of A_o proves important for the stress-dilatancy and the stress-strain relation in Figs. 7(a and b), respectively. The significant effect of A_o in Fig. 7(a) is expected, since the calculated $d\varepsilon_p^p$ is analogous to the dilatancy coefficient A_o [see (6*b*) and (16)]. The corresponding effect of dilatancy (via A_o) on the stress-strain relation is shown in Fig. 7(b), while Fig. 7(c) shows that varying h_o does not affect dramatically the simulated stress-strain relation. These results agree with Li and Dafalias (2000), who studied the effect of dilatancy on a theoretical basis. Their study shows that when the stress state has practically converged to the bounding surface (as in the shearing paths in Fig. 7) the stress-strain relation is practically governed by dilatancy (hence A_o) and not the plastic modulus K_p (hence h_o). To avoid misconceptions, note that when the stress state is far from the bounding surface the actual value of h_o becomes important for the stress-strain relation.

Similarly, Fig. 8 presents a parametric analysis for the effect of F_o and X on the simulated cyclic drained triaxial behavior with emphasis on volume change. Solid lines correspond to model simulations performed with the parameters of Table 1 for cyclic shearing, while the dashed lines correspond to the noted parametric sensitivity runs. Observe that an increase in both parameters results in a stiffer response.

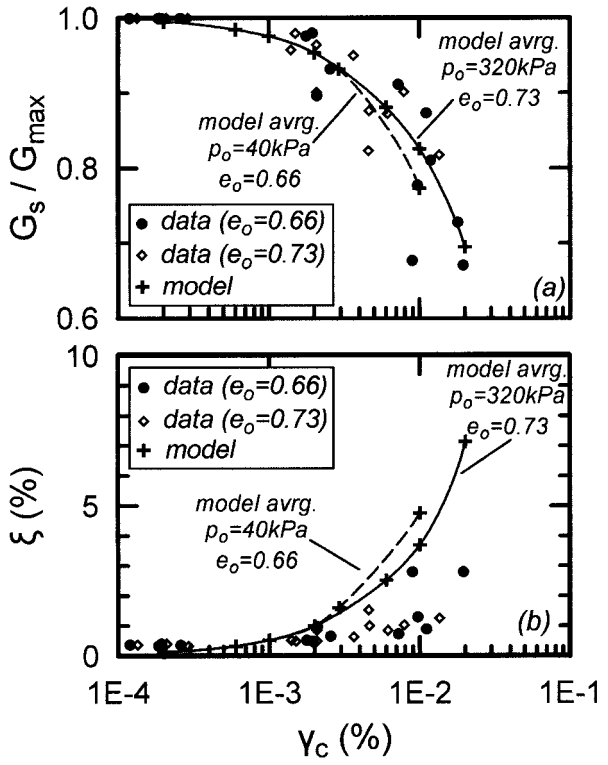

FIG. 9. Summary Comparison of Model Simulations to Resonant Column Test Data of Nevada Sand: (a) G_s/G_{max}-γ_c; (b) ξ-γ_c

EVALUATION OF MODEL PERFORMANCE

To assess model performance under widely variable initial, shearing, and drainage conditions, a total of 47 cyclic shearing tests are used. These include resonant column and cyclic liquefaction tests on Nevada sand (Arulmoli et al. 1992) as well as cyclic drained tests on Oosterschelde sand [Massachusetts

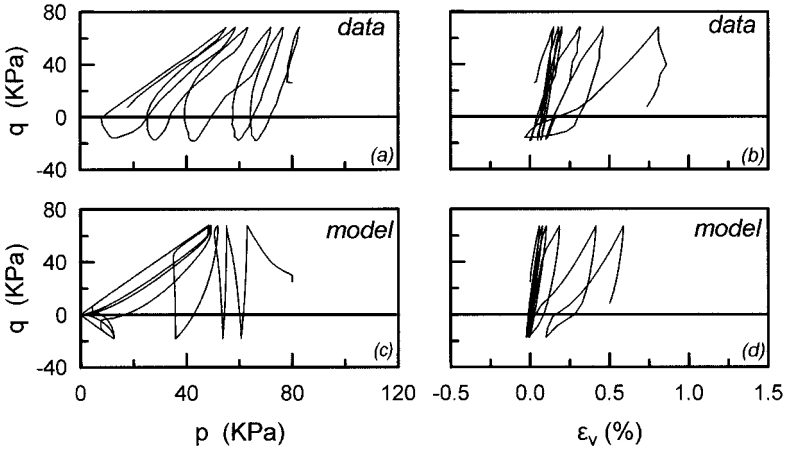

FIG. 10. Detailed Comparison of Model Simulations to Data from Cyclic Liquefaction Triaxial Test on Nevada Sand: (a and c) Effective Stress Path; (b and d) Stress-Strain Relation (Calibration Test 1)

Institute of Technology (MIT) 1979]. Note that the Nevada sand tests can be divided into two groups, those having initial void ratios $e_o \cong 0.66$ and those with $e_o \cong 0.73$. On the other hand, the Oosterschelde sand samples had initial void ratios ranging uniformly from 0.70 to 0.77. Using data from different sands is unavoidable, given that an all-inclusive test database was not found in the reviewed literature. All pertinent simulations are performed with the parameter values for cyclic shearing of Nevada sand in Table 1. Hence, Oosterschelde sand is assumed to behave similarly to Nevada sand, a hypothesis justified by the comparable gradations of the two soils.

Resonant Column Tests

Fig. 9 presents summary comparisons of model simulations to data from 15 resonant column tests, which were performed for p_o = 40, 80, 160, and 320 kPa. Given that the effect of initial conditions on G_{max} has been accurately considered in the calibration of the elastic shear modulus parameters [Fig. 6(a)], test data and simulations are presented in summary plots of G_s/G_{max}-γ_c and ξ-γ_c. In particular, circular and rhombic symbols in Fig. 9 correspond to test data, while the dashed and solid lines denote estimates of the upper and lower bounds of the simulated G_s/G_{max}-γ_c and ξ-γ_c curves for the initial conditions at hand. These estimates are based on example simulations marked by crosses in this figure. Observe that the analytical simulations in Fig. 9(a) provide a satisfactory fit of the scattered data for G_s/G_{max} degradation, regardless of initial conditions. On the other hand, the respective damping ratio ξ values are slightly overestimated in Fig. 9(b). However, this overestimation can be attributed to the fact that the pertinent

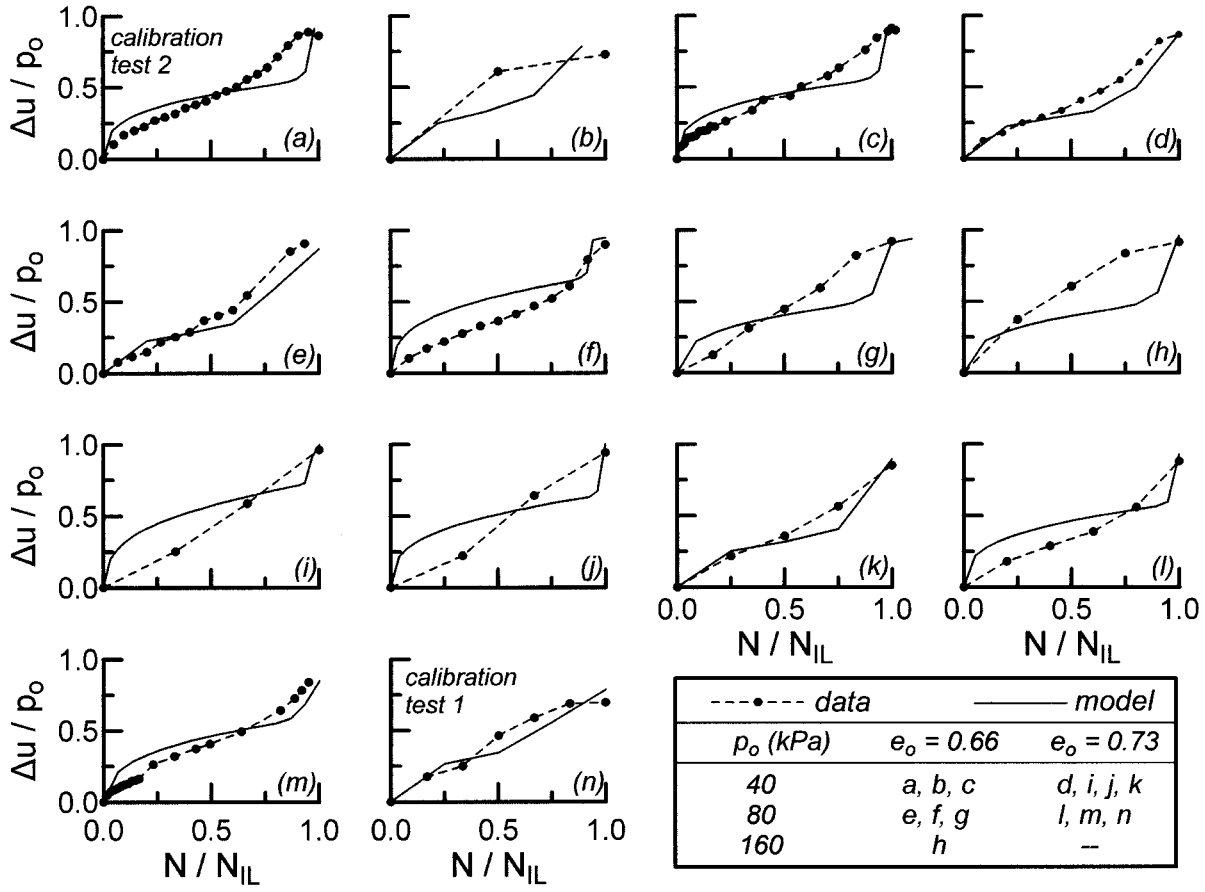

FIG. 11. Summary Comparison of Simulated and Measured Average Rates of Excess Pore Pressure Δu Buildup from 14 Cyclic Liquefaction Triaxial Tests on Nevada Sand, Including Denoted Calibration Tests 1 and 2

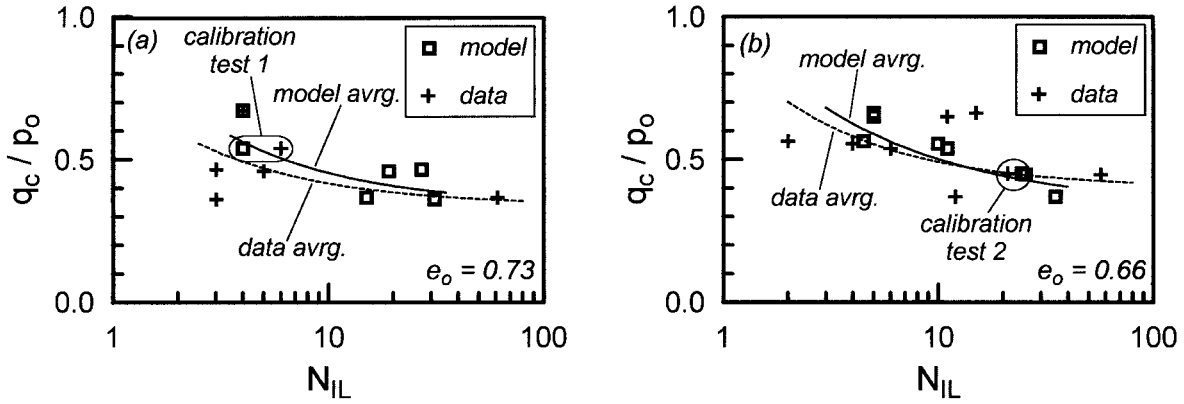

FIG. 12. Average Liquefaction Curves Deduced from Simulations and Data from 14 Cyclic Liquefaction Triaxial Tests on Nevada Sand: (a) $e_o \cong 0.73$; (b) $e_o \cong 0.66$ (Calibration Tests Are Appropriately Denoted)

measurements are unusually low compared with empirical ξ-γ_c curves for sands from the literature [e.g., Vucetic and Dobry (1991)].

Cyclic Liquefaction Tests

Fig. 10 compares the measured stress path and stress-strain relation to their simulations in one of the two cyclic liquefaction tests on Nevada sand that were used for calibration (Test 1). It is observed that the model simulates test measurements well, even in the generally hard to simulate area of initial liquefaction, where p is near zero. This accuracy extends to both the stress path and the deviatoric stress-strain relation.

For a more global estimate of accuracy in simulating excess pore pressure buildup and liquefaction under variable initial and shearing conditions with the same set of parameters, Fig. 11 presents a summary comparison of simulations and test data from 14 liquefaction tests, including the denoted calibration tests (Tests 1 and 2). The presentation refers to the evolution of the average rate of excess pore pressure Δu buildup with the number of load cycles N. To enable comparison between tests of different conditions, the Δu value is normalized to the initial mean effective stress p_o, while the number of cycles N is normalized to the number of cycles to initial liquefaction N_{IL} of each test. On the whole, simulations are in good gross agreement with experimental data.

To draw the full picture, a comparison between measured and simulated liquefaction resistance in all 14 tests is presented in Fig. 12. In particular, liquefaction resistance is quantified in terms of the number of cycles to initial liquefaction N_{IL} for different densities. Observe that despite the considerable scatter of test results the average liquefaction curves procuring from the simulations are similar to the ones based on the test data. Furthermore, observe that the model simulates the experimentally established increase in liquefaction resistance with density.

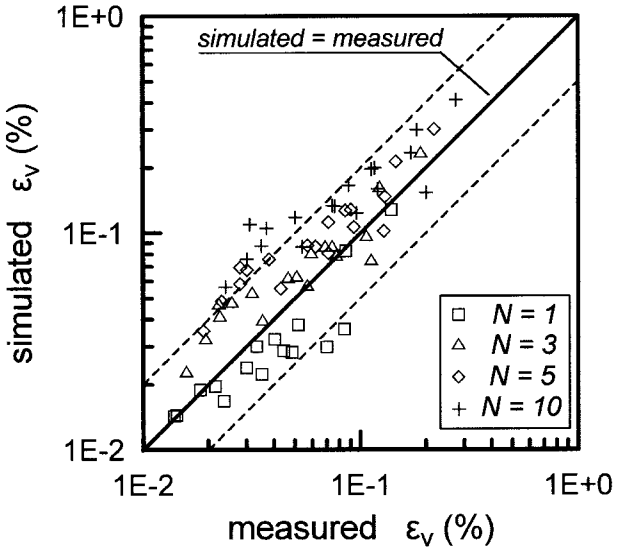

FIG. 13. Summary Comparison of Simulated and Measured Values of Accumulated Vertical (Axial) Strain ε_v after N = 1, 3, 5, and 10 Cycles of Drained Triaxial Tests on Oosterschelde Sand

Drained Cyclic Tests

Fig. 13 presents a summary comparison of simulated and measured values of accumulated vertical (axial) strain ε_v after N = 1, 3, 5, 10 in 18 drained cyclic triaxial tests. More specifically, each symbol in Fig. 13 corresponds to a different test and is obtained, on one hand, using as coordinates the test measurement after a specific number of load cycles N, and, on the other hand, the respective simulated value of accumulated ε_v. The solid diagonal line is the locus of points of perfect agreement between simulations and measurements, while the two dashed lines denote the loci of overestimation and underestimation by a factor of 2. It is observed that, on the whole, the simulations agree well with the test data.

Monotonic Tests

Despite that emphasis in this article is on cyclic shearing, it is of practical importance to ascertain whether monotonic shearing can be accurately simulated as well. Thus, Fig. 14 presents comparisons of model simulations to test data from six monotonic triaxial compression tests on Nevada sand. Specifically, Fig. 14(a) refers to the results of deviatoric stress q versus vertical (axial) strain ε_v of three undrained tests with $e_o \cong 0.66$ and mean effective consolidation stress p_o = 40, 80, and 160 kPa. Similarly, Fig. 14(b) refers to the results of volumetric strain ε_p versus vertical (axial) strain ε_v of three drained constant-p tests with $e_o \cong 0.73$ and the same consolidation stresses. Note that the test results for p_o = 80 kPa were used as target stress-strain response during the calibration procedure. This figure establishes that the model simulates the experiments reasonably well for all densities and mean effective consolidation stresses.

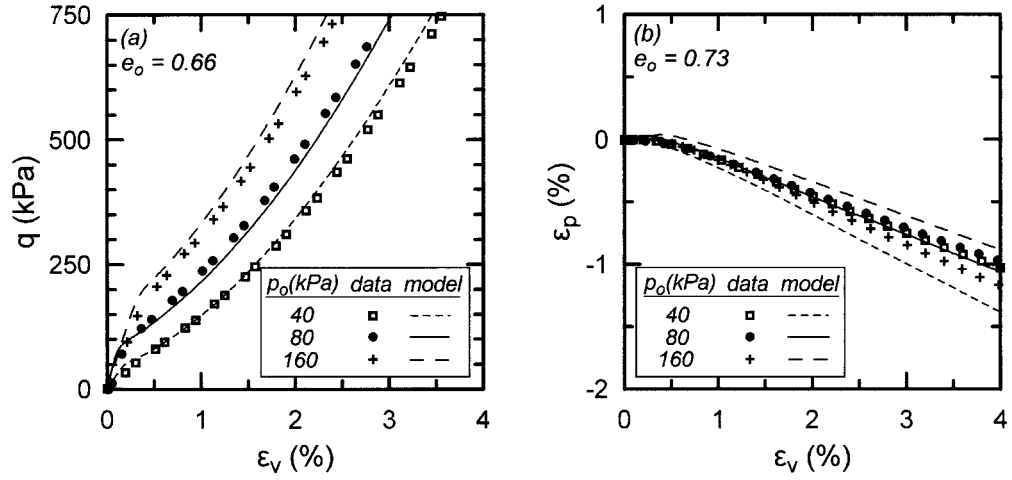

FIG. 14. Summary Comparison of Simulations to Data from Monotonic Triaxial Compression Tests on Nevada Sand under: (a) Undrained Conditions; (b) Drained Conditions (Data for p_o = 80 kPa Were Used for Calibration)

CONCLUSIONS

This paper presents a yield/bounding surface critical state constitutive model built with the aim to provide accurate simulations for the cyclic response of sands under small as well as large cyclic strains, irrespective of initial density and mean effective stress levels.

The formulation builds on the recently proposed model of Manzari and Dafalias (1997) and introduces two new key elements: (1) a nonlinear hysteretic type of behavior for small cyclic strains in a paraelastic manner; and (2) a scalar-valued fabric evolution variable in the definition of the plastic modulus, which improves simulation of cyclic response under large cyclic strains. In effect, what these two constitutive ingredients achieve is to incorporate practical geotechnical experience into an efficient analytical framework.

To provide the assessment required for practical applications, model evaluation is not limited to one-to-one simulations of a few element tests, as normally done in practice. More specifically, data from 15 resonant column and 32 cyclic triaxial tests of variable initial, shearing, and drainage conditions are compared to model simulations performed with a single set of parameters. A good agreement of simulations and experimental data is observed for the majority of these tests, which correspond to both small and large cyclic shear strain levels. Accurate simulation of monotonic shearing proves possible, given an adjustment to the value of 1 out of the 14 parameters.

ACKNOWLEDGMENTS

The support of this research by the State Fund Institution of Greece (IKY) is gratefully acknowledged. In addition, Y. F. Dafalias acknowledges support by the National Science Foundation Grant CMS-9800330. The help of Dr. M. Jefferies, who supplied useful data on sands, is appreciated.

REFERENCES

Arthur, J. R. F., Bekenstein, S., Germaine, J. T., and Ladd, C. C. (1981). ''Stress path tests with controlled rotation of principal stress directions.'' *Laboratory shear strength of soil, ASTM STP 740*, ASTM, West Conshohocken, Pa.

Arulmoli, K., Muraleetharan, K. K., Hossain, M. M., and Fruth, L. S. (1992). ''VELACS: Verification of liquefaction analyses by centrifuge studies; laboratory testing program—Soil data report.'' *Res. Rep.*, The Earth Technology Corp.

Been, K., and Jefferies, M. G. (1985). ''A state parameter for sands.'' *Géotechnique*, London, 35(2), 99–112.

Chen, Y.-C., Ishibashi, I., and Jenkins, J. T. (1988). ''Dynamic shear modulus and fabric: Part I, Depositional and induced anisotropy.'' *Géotechnique*, London, 38(1), 25–32.

Dafalias, Y. F., and Popov, E. P. (1975). ''A model of nonlinearly hardening materials for complex loadings.'' *Acta Mechanica*, 21, 173–192.

Egglezos, D. N., and Bouckovalas, G. D. (1999). ''Permanent strain and pore pressure relations for cyclic loading of sand.'' *Proc., 2nd Int. Conf. on Earthquake Geotech. Engrg.*, Vol. 1, 131–136.

Gajo, A., and Wood, D. M. (1999). ''A kinematic hardening constitutive model for sands: The multiaxial formulation.'' *Int. J. Numer. and Analytical Methods in Geomech.*, 23, 925–965.

Hardin, B. O. (1978). ''The nature of stress-strain behavior for soils.'' *Proc., ASCE Spec. Conf. on Earthquake Engrg. and Soil Dyn., State-of-the-art Rep.*, ASCE, New York, 3–90.

Hueckel, T., and Nova, R. (1979). ''Some hysteresis effects of the behavior of geological media.'' *Int. J. Solids and Struct.*, 15, 625–642.

Ishihara, K., Tatsuoka, F., and Yasuda, S. (1975). ''Undrained deformation and liquefaction of sand under cyclic stresses.'' *Soils and Found.*, Tokyo, 15(1), 29–44.

Jefferies, M. G. (1993). ''Nor-Sand: A simple critical state model for sand.'' *Géotechnique*, London, 43(1), 91–103.

Jefferies, M. G., and Been, K. (1987). ''Use of critical state representations of sand in the method of characteristics.'' *Can. Geotech. J.*, Ottawa, 24(3), 441–446.

Ladd, C. C., Foott, R., Ishihara, K., Schlosser, F., and Poulos, H. G. (1977). ''Stress-deformation and strength characteristics.'' *Proc., 9th Int. Conf. on Soil Mech. and Found. Engrg., State-of-the-art rep.*, Vol. 2, 421–494.

Li, X. S., and Dafalias, Y. F. (2000). ''Dilatancy for cohesionless soils.'' *Géotechnique*, London, 50(4), 449–460.

Li, X. S., Dafalias, Y. F., and Wang, Z. L. (1999). ''State-dependent dilatancy in critical-state constitutive modelling of sand.'' *Can. Geotech. J.*, Ottawa, 36(4), 599–611.

Manzari, M. T., and Dafalias, Y. F. (1997). ''A critical state two-surface plasticity model for sands.'' *Géotechnique*, London, 47(2), 255–272.

Massachusetts Institute of Technology (MIT). (1979). ''Cyclic triaxial tests on Oosterschelde sands.'' *Res. Rep. R79-24, Soils Publ. No. 646*, Department of Civil Engineering, Cambridge, Mass.

Oda, M., Nemat-Nasser, S., and Konishi, J. (1985). ''Stress-induced anisotropy in granular materials.'' *Soils and Found.*, Tokyo, 25(3), 85–97.

Papadimitriou, A. G. (1999). ''Elastoplastic modeling of monotonic and dynamic behavior of soils.'' Doctorate thesis, Geotech. Div., National Technical University of Athens, Athens, Greece (in Greek).

Papadimitriou, A. G., Bouckovalas, G. D., and Dafalias, Y. F. (1999). ''Use of elastoplasticity to simulate cyclic sand behavior.'' *Proc., 2nd Int. Conf. on Earthquake Geotech. Engrg.*, Vol. 1, 125–130.

Popescu, R., and Prevost, J. H. (1995). ''Comparison between VELACS numerical 'Class A' simulations and centrifuge experimental soil test results.'' *Soil Dyn. and Earthquake Engrg.*, 14(2), 79–92.

Ramberg, W., and Osgood, W. R. (1943). ''Description of stress-strain curve by three parameters.'' Technical Note 902, National Advisory Committee for Aeronautics, Washington, D.C.

Schofield, A. N., and Wroth, C. P. (1968). *Critical state soil mechanics*, McGraw-Hill, London.

Seed, H. B., and Booker, J. R. (1977). ''Stabilization of potentially liquefiable sand deposits.'' *J. Geotech. Engrg. Div.*, ASCE, 103(7), 757–768.

Tatsuoka, F., and Ishihara, K. (1974). ''Drained deformation under cyclic stresses reversing direction.'' *Soils and Found.*, Tokyo, 14(3), 51–65.

Vucetic, M. (1994). ''Cyclic threshold shear strains in soils.'' *J. Geotech. Engrg.*, ASCE, 120(12), 2208–2228.

Vucetic, M., and Dobry, R. (1991). ''Effect of soil plasticity on cyclic response.'' *J. Geotech. Engrg.*, ASCE, 117(1), 89–107.

Wood, D. M., Belkheir, K., and Liu, D. F. (1994). ''Strain softening and state parameter for sand modelling.'' *Géotechnique*, London, 44(2), 335–339.